Atmos. Meas. Tech., 9, 2179–2194, 2016
www.atmos-meas-tech.net/9/2179/2016/
doi:10.5194/amt-9-2179-2016

Atmospheric Measurement Techniques
Open Access
EGU

An optical particle size spectrometer for aircraft-borne measurements in IAGOS-CARIBIC

Markus Hermann[1], Andreas Weigelt[1,2,a], Denise Assmann[1], Sascha Pfeifer[1], Thomas Müller[1], Thomas Conrath[1], Jens Voigtländer[1], Jost Heintzenberg[1], Alfred Wiedensohler[1], Bengt G. Martinsson[3], Terry Deshler[4], Carl A. M. Brenninkmeijer[5], and Andreas Zahn[6]

[1]Leibniz Institute for Tropospheric Research, Permoserstr. 15, 04318 Leipzig, Germany
[2]Environmental Chemistry Department, Helmholtz-Zentrum Geesthacht, Max-Planck-Straße 1, 21502 Geesthacht, Germany
[3]Division of Nuclear Physics, Lund University, Professorsgatan 1, 22363 Lund, Sweden
[4]Department of Atmospheric Science, University of Wyoming, 1000 E. University Avenue, Laramie, WY 82071, USA
[5] Air Chemistry Division, Max Planck Institute for Chemistry, Hahn-Meitner-Weg 1, 55128 Mainz, Germany
[6]Institute for Meteorology and Climate Research, Karlsruhe Institute of Technology, Hermann-von-Helmholtz-Platz 1, 76344 Eggenstein-Leopoldshafen, Germany
[a]now at: Federal Maritime and Hydrographic Agency, Wuestland 2, 22589 Hamburg, Germany

Correspondence to: Markus Hermann (hermann@tropos.de)

Received: 11 September 2015 – Published in Atmos. Meas. Tech. Discuss.: 4 November 2015
Revised: 8 March 2016 – Accepted: 22 March 2016 – Published: 17 May 2016

Abstract. The particle number size distribution is an important parameter to characterize the atmospheric aerosol and its influence on the Earth's climate. Here we describe a new optical particle size spectrometer (OPSS) for measurements of the accumulation mode particle number size distribution in the tropopause region on board a passenger aircraft (IAGOS-CARIBIC observatory: In-service Aircraft for a Global Observing System – Civil Aircraft for Regular Investigation of the Atmosphere Based on an Instrument Container). A modified KS93 particle sensor from RION Co., Ltd., together with a new airflow system and a dedicated data acquisition system, is the key component of the CARIBIC OPSS. The instrument records individual particle pulse signal curves in the particle size range 130–1110 nm diameter (for a particle refractive index of 1.47-i0.006) together with a time stamp and thus allows the post-flight choice of the time resolution and the size distribution bin width. The CARIBIC OPSS has a 50 % particle detection diameter of 152 nm and a maximum asymptotic counting efficiency of 98 %. The instrument's measurement performance shows no pressure dependency and no particle coincidence for free tropospheric conditions. The size response function of the CARIBIC OPSS was obtained by a polystyrene latex calibration in combination with model calculations. Particle number size distributions measured with the new OPSS in the lowermost stratosphere agreed within a factor of 2 in concentration with balloon-borne measurements over western North America. Since June 2010 the CARIBIC OPSS is deployed once per month in the IAGOS-CARIBIC observatory.

1 Introduction

The particle number size distribution is essential to describe the physical properties of the atmospheric aerosol and its influence on climate (Charlson et al., 1992; Mann et al., 2014). In particular in the accumulation mode (particles with diameters of 0.1–1.0 µm) this information is of interest, because this mode dominates the particle surface area concentration in most cases and thus the radiative properties of the atmospheric aerosol (Seinfeld and Pandis, 1998). Moreover the accumulation mode dominates the total particle mass concentration in air masses without coarse mode particles (particle diameter larger than 1.0 µm), for instance in the upper troposphere and lowermost stratosphere (UT/LMS). Aerosol particles in this region provide surface area for heterogeneous chemistry (Søvde et al., 2007) and influence the formation of ice clouds (Krämer et al., 2009) and thereby in-

directly impact the Earth's radiation budget. The discovery of the Asian Tropopause Aerosol Layer (ATAL) by Vernier et al. (2011) and the much stronger than previously thought radiative impact of volcanic aerosols in the UT/LMS (Andersson et al., 2015) are just two examples of the importance, but also the limited knowledge, of the UT/LMS aerosol.

Particle number size distribution can be sensed either remotely or in situ. Remote sensing methods have the advantage of providing vertical information (e.g., by lidars) or near-global coverage (by satellite instruments). However, particle number size distributions derived from remote sensing methods bear large uncertainties. Furthermore, in the free troposphere, where the aerosol mass load usually is low, some instruments have problems identifying aerosol signals because of their detection limits (Winker et al., 2013). In situ particle number size distribution measurements give the most detailed information and can be used to validate remote sensing results. Commonly used are mobility particle size spectrometers (MPSSs; Wiedensohler et al., 2012) and optical particle size spectrometers (OPSSs; Gebhart, 2001). An OPSS, as discussed in this paper, measures the light scattered by individual particles to derive their number and diameters. The relationship between particle diameter and scattered light is mostly established in the laboratory usually by calibration with polystyrene latex (PSL) particles. For aircraft-borne measurements, OPSSs are preferably used (e.g., de Reus et al., 2000, 2001; Krejci et al., 2003; Schröder et al., 2002; Young et al., 2007; Zaizen et al., 2004) because they can measure relatively fast and do not have problems with the aviation permission (in contrast to MPSS systems with radioactive chargers). However, calibration of OPSSs, as described here, is always an issue (e.g., Rosenberg et al., 2012; Cai et al., 2013) because of the effects of particle refractive index and shape.

Aside from the long-term balloon-borne measurement series at Laramie, Wyoming (Deshler et al., 2003), there have been no regular in situ measurements of the accumulation mode particle number size distribution in the UT/LMS. In this study we present a new OPSS applied for regular measurements of the UT/LMS particle number size distribution on board a passenger aircraft. Particle size distributions measured by this OPSS were already used in previous studies (Rauthe-Schöch et al., 2012; Martinsson et al., 2014; Andersson et al., 2015), but here the instrument is described in detail for the first time (Sect. 2). The new OPSS was thoroughly characterized in the laboratory with respect to particle pulse signals, pressure dependency, particle sizing, particle counting efficiency, and particle coincidence (Sect. 3). A post-flight data processing routine was developed and measurement uncertainties were assessed (Sect. 4). Since June 2010 the OPSS is operated on two to four intercontinental flights per month as part of the scientific payload on board a Lufthansa Airbus A340-600 within the CARIBIC (Civil Aircraft for Regular Investigation of the Atmosphere Based on an Instrument Container; www.caribic-atmospheric.com, accessed 1 July 2015, and Brenninkmeijer et al., 2007) part of the European research infrastructure IAGOS (In-service Aircraft for a Global Observing System; www.iagos.org, accessed 1 July 2015). Examples of two flights provide an impression of the UT/LMS aerosol data obtained (Sect. 5).

2 CARIBIC OPSS description

2.1 Original instrument: the RION particle sensor KS-93

Although the CARIBIC measurement container weighs 1.6 tons and is 3 m wide, the large number of on-board experiments forces a focus on small and light equipment with low power consumption. Besides these constraints we required an instrument with a lower size detection limit below 200 nm equivalent optical particle diameter. These requirements are fulfilled by the KS-93 particle sensor (RION CO., Ltd., Japan; www.rion.co.jp/english/, accessed 1 July 2015), an instrument developed for semiconductor manufacturing applications, which had not been applied to airborne atmospheric research before. The KS-93 particle sensor is light (6.5 kg) and small (135 mm $\times$ 280 mm $\times$ 150 mm) and has a robust synthetic quartz optical cell, which makes it well suited for airborne aerosol research. The KS-93 optics uses perpendicular polarized light from a diode laser with 830 nm wavelength and a light detection system at $90\pm40^\circ$ collecting angle. The manufacturer specifies particle number concentration measurements in five size bins between 0.1 and 2.0 µm optical particle diameter with 50 % counting efficiency. To cover the whole particle signal range of more than 4 orders of magnitude, the KS-93 uses three linear amplifiers. In order to increase the number of size bins by using a new data acquisition, it was necessary to directly access the scattered light signals. Therefore RION modified one KS93 for CARIBIC and installed three new SMB (miniature coaxial radio frequency) connectors at the KS-93 rear plate, which allow direct access to the particle signals of the three amplifiers. The volume flow through the KS-93 can be varied between 0.05 and 0.3 L min^{-1} and must be externally controlled.

2.2 CARIBIC OPSS

The modified KS-93 is mounted together with the flow control system and the new data acquisition in a 19 in. electromagnetic compatibility (EMC) rack unit (Fig. 1, chassis: Knürr). As the aerosol inlet and outlet of the KS-93 are glued to the quartz optical cell inside the KS-93, the instrument is somewhat sensitive to shocks and vibration. Therefore the modified KS-93 was mounted in a dedicated aluminum frame, which is fixed on the ground plate by three wire rope isolators (Enidine, Orchard Park, NY, USA). Because of this construction, all air tubing to the modified KS-93 (electroconductive silicone tubing with 4.83 mm inner diameter; TSI, Shoreview, MN, USA), as well as power and

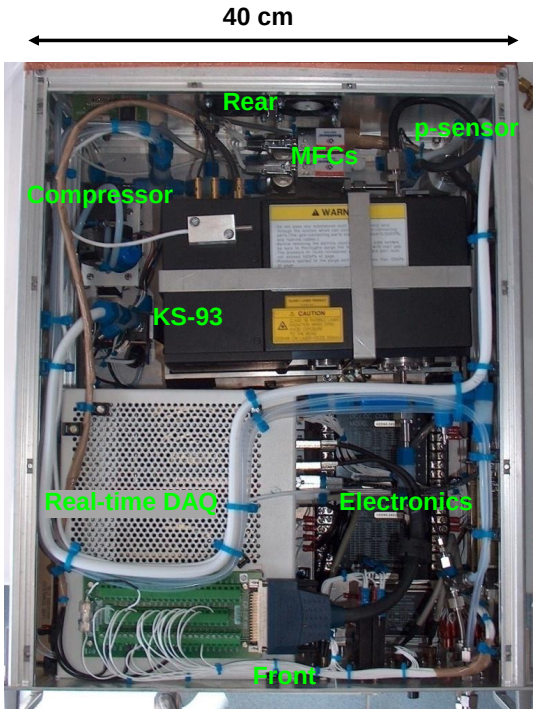

Figure 1. Top view of the CARIBIC optical particle size spectrometer (OPSS).

signal cables, is flexibly connected. Besides the modified KS-93, the CARIBIC OPSS houses electronic components (EMI filter, DC/DC converters) and a flow control system (mass flow controllers, compressor, as well as temperature and pressure sensors). Access to the CARIBIC OPSS is provided via the front plate, where the power and communication connectors are located. In the rear plate, the CARIBIC OPSS has a compact flash data card slot, where the measurement data are stored and can be accessed. The sample air enters the CARIBIC OPSS through the front plate and leaves the instrument through the rear plate, where a vacuum source must be applied. For CARIBIC this is a common diaphragm pump (Vaccubrand) in another rack unit, used for all CARIBIC aerosol instruments, including three condensation particle counters (CPCs) (Hermann and Wiedensohler, 2001) and an aerosol particle impactor sampler (Nguyen et al., 2006).

To obtain the aeronautic certification for the aircraft, all materials must be nonflammable (e.g., Teflon-covered cables) and all fasteners secured against loosening. Moreover, the CARIBIC OPSS had to pass an EMC test (RTCA DO-160E) to ensure that it does not interfere with the aircraft electronic systems.

A schematic of the CARIBIC OPSS sample and auxiliary airflow system is shown in Fig. 2. There are two basic operating states. In the stand-by mode (green arrows in Fig. 2), about $3\,\mathrm{L\,min^{-1}}$ of filtered air originating from the diaphragm compressor (KNF Neuberger) leaves the two-way selector valve via port 1. As both mass flow controllers (MFCs; Bronkhorst) are closed and the external vacuum pump is not switched on, the $3\,\mathrm{L\,min^{-1}}$ is pushed through the flow splitter and the sample air inlet out of the CARIBIC OPSS and into the aerosol inlet system in the aircraft. This purging mechanism is in operation during aircraft takeoff and landing to prevent contamination of the sampling line and all aerosol instruments by polluted air in the vicinity of airports.

In measuring mode (blue arrows in Fig. 2) the two-way selector valve is switched and the particle-free air from the compressor is now directed through port 2. At the same time the external vacuum pump is switched on. In this mode, particle-free sheath air is applied around the aerosol sampling air by adjusting MFC1 to $0.150\,\mathrm{L\,min^{-1}}$ and MFC2 to $0.134\,\mathrm{L\,min^{-1}}$ (see Sect. 3.2). Using the pressure and the temperature data from the sensors in the airflow, the MFCs are adjusted to a constant volume flow through the optics by a 1 Hz LabVIEW proportional–integral–derivative (PID) controller algorithm. This measure guarantees for each MFC a constant air volume flow with 1 % accuracy despite pressure changes during flight. MFC2 provides only 90 % of the air drawn through the optics to the vacuum (the sheath air). The residual sample airflow of $0.016\,\mathrm{L\,min^{-1}}$ is taken from the CARIBIC aerosol inlet via a flow splitter and the sheath air device upstream of the KS-93 optics. To reduce the residence time of the sample air in the sampling line between the inlet at the aircraft fuselage and the aerosol instruments in the container a volume flow close to the laminar limit is applied ($\sim 20\,\mathrm{L\,min^{-1}}$). To minimize wall effects the core flow is transported to the aerosol units using a first flow splitter (not shown). The particle-depleted air near the tubing wall (flow splitter excess air, $\sim 4\,\mathrm{L\,min^{-1}}$) is drawn to the vacuum. This excess airflow is controlled by a critical orifice. From the first flow splitter about $1\,\mathrm{L\,min^{-1}}$ of measurement air is drawn through a 1 m long 0.25 in. tubing to the second flow splitter inside the CARIBIC OPSS. At the second flow splitter, which is located about 10 cm upstream of the sheath air insertion point, again only the less influenced core flow ($0.016\,\mathrm{L\,min^{-1}}$) is utilized for the particle measurement. The rest, the OPSS excess air, is drawn to the vacuum, again controlled by a critical orifice. The pressure of the external vacuum is monitored in another aerosol rack unit and always remains below 40 % of the operation pressure at the CARIBIC OPSS inlet, thus ensuring proper critical orifice flow control.

2.3 Data acquisition and unit control

In the KS-93 particle sensor the scattered light from each particle is sensed by a photodiode and the respective particle signal is amplified in parallel by the three internal linear amplifiers. In the CARIBIC OPSS the output of these amplifiers is recorded with a real-time data acquisition system (PXI, National Instruments) with 3 µs time resolution. As the original pulse of a single particle has a duration of about 60–150 µs (see Fig. 4), each pulse is thus resolved with 20–

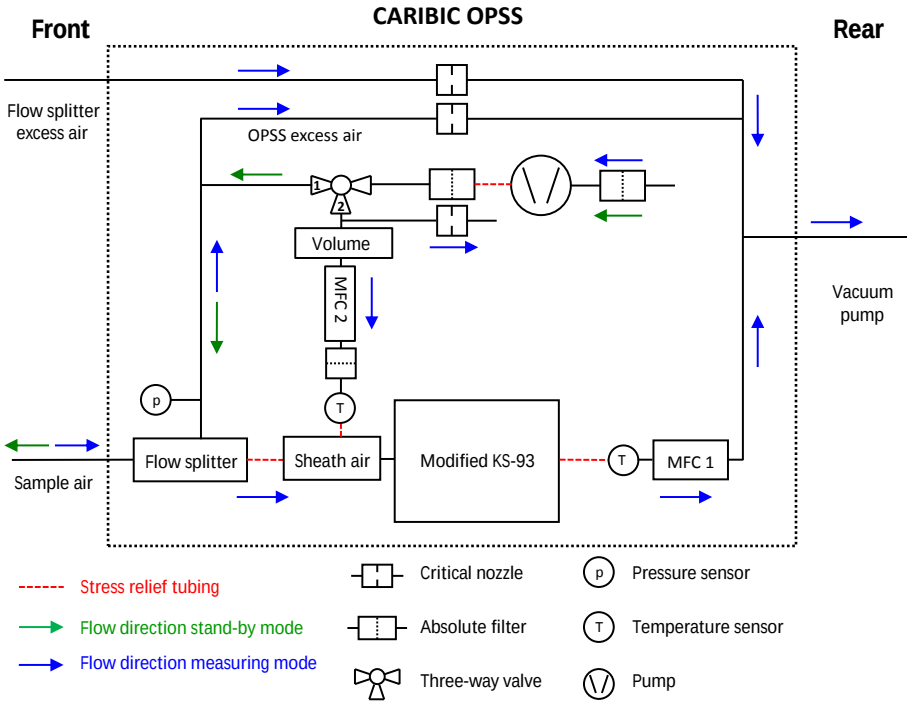

Figure 2. Air flow diagram of the CARIBIC OPSS.

50 data points. The full-width half maximum of the amplified particle signals is about 30 µs for all particle diameters. This data acquisition allows a flexible choice of the averaging time and number of size bins during post-flight processing. In addition, since the complete pulse shape is preserved, additional filtering can be applied to suspect particles that might have passed through less-than-optimum regions of the laser beam. For the current version of the CARIBIC OPSS data (V14) particle pulse height maxima are sorted into 10 size bins and averaged over 180 s. Besides the particle signals, the data acquisition also records housekeeping data (operating pressure, measurement air and unit temperatures, and mass flows) with 10 Hz resolution. All routines are written in LabVIEW (National Instruments).

The CARIBIC container is a fully automated flying observation laboratory (see Brenninkmeijer et al., 2007). For safety and power management reasons the container and its instruments are controlled by a master computer via an internal network. Thus, the LabVIEW program written for the CARIBIC OPSS includes a communication routine that follows the CARIBIC communication protocol and determines the operating status of the CARIBIC OPSS. The OPSS communication with the master is restricted to simple control commands and answers, whereas the particle signal data are solely stored in the CARIBIC OPSS.

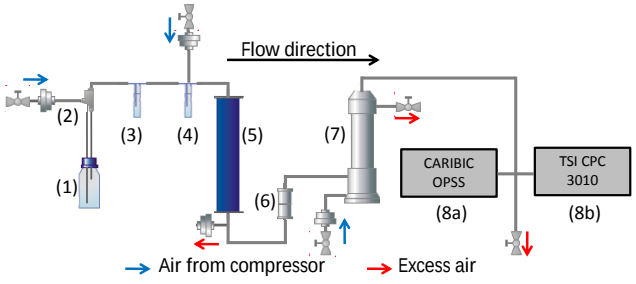

Figure 3. OPSS calibration setup with (1) glass bottle containing the particle material in aqueous solution or suspension, (2) particle generator (nebulizer), (3) droplet trap, (4) dilution unit, (5) silica gel drier, (6) bipolar diffusion charger, and (7) a differential mobility analyzer. A TSI condensation particle counter (CPC 3010) was operated in parallel to the CARIBIC OPSS (8a and 8b) as reference for the counting efficiency measurements.

3 CARIBIC OPSS characterization

3.1 OPSS calibration setup

For the calibration of the CARIBIC OPSS with respect to particle size and counting efficiency, measurements with different particle sizes were carried out using the setup shown in Fig. 3. The particle material (PSL or ammonium sulfate, AS) was suspended in deionized water (1). After nebulizing this suspension in a TSI 3076 particle generator (nebulizer) (2), the aerosol was directed into a droplet trap (3). While large

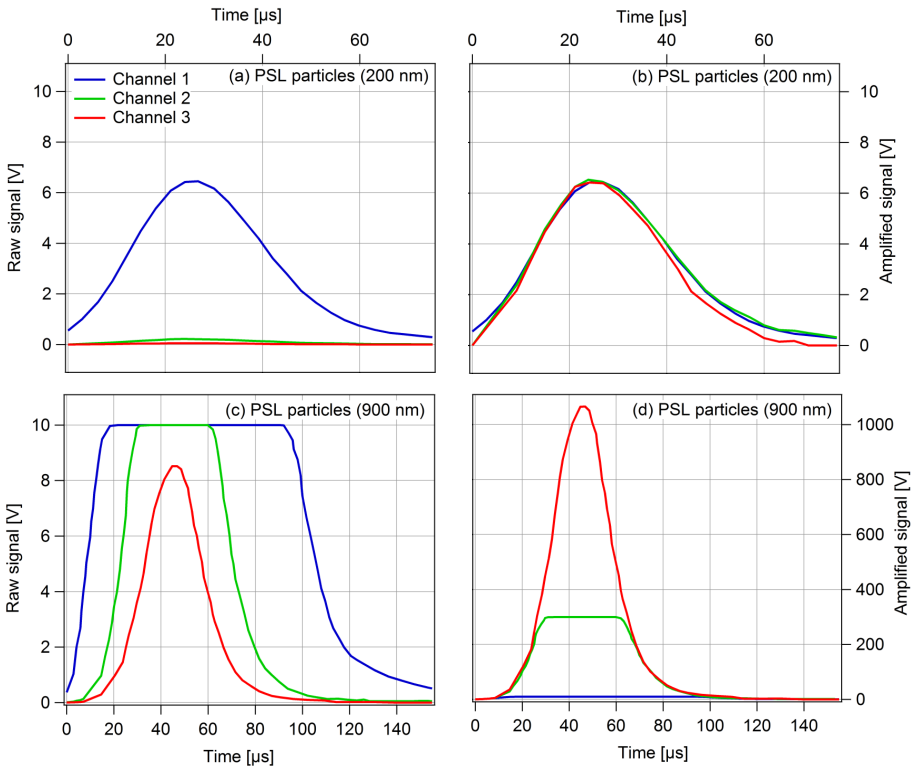

Figure 4. Particle signal pulses measured with all three CARIBIC OPSS channels for 200 and 900 nm diameter polystyrene latex (PSL) particles. **(a)** and **(c)** show the raw signals at the SMB connectors of the modified KS-93. The amplified signals (factor of 30 for Ch2 and 125 for Ch3), used for data analysis, are shown in **(b)** and **(d)**, respectively.

droplets were removed by impaction, the small ones followed the air stream into a glass bottle dilution unit (4). In this glass bottle the calibration air was mixed with dry particle-free air to reduce the total particle number concentration and to dry the droplets. By adjusting the dilution ratio the particle number concentration of the measurement air was set between 20 and 1000 cm^{-3}. To obtain really dry particles, the aerosol passed an additional silica-filled diffusion drier (5). When PSL calibration standards (Duke Scientific Corporation, Nanosphere size standards NIST traceable mean diameter, Thermo Fisher Scientific) were used, the resulting particle number size distribution downstream of the drier was quasi-monodisperse. However, some particles, much smaller than the specified PSL particle diameter, were present due to the remaining impurity of the nebulized water ("water peaks"). Therefore the quasi-monodisperse PSL particles were charged inside a bipolar diffusion charger (Am^{241}) (6) and size-separated using a differential mobility analyzer (DMA; Vienna type) (7). Downstream of the DMA the monodisperse PSL aerosol was directed to the CARIBIC OPSS (8a). The reference instrument for the particle number concentration was a CPC (TSI model 3010, 8b), which has the same volume flow rate of 1 L min^{-1} as the CARIBIC OPSS. Particle losses due to sedimentation, impaction, and diffusion were minimized by avoiding strong tube bends and keeping the tubing as short as possible. For the determination of the CARIBIC OPSS counting efficiency, particles with many different particle diameters were needed; hence, AS particles were generated in a similar way, as described for PSL above.

3.2 OPSS particle pulse signals

To record individual pulse signals, the KS-93 amplifier outputs are connected to the newly installed SMB connectors, called channels one to three (Ch1–3). The amplified particle pulses have roughly a Gaussian shape and amplitudes of 0–10 V (Fig. 4). Ch1 has the highest gain to resolve the signals of particles smaller than about 234 nm diameter (with respect to an UT particle refractive index of 1.47-i0.006; see Sect. 3.4). Particles larger than about 234 nm and smaller than about 515 nm are resolved best with the second channel (Ch2). All larger aerosol particles are resolved only in the third channel (Ch3). The upper limit of Ch3 and therefore the upper limit for size-resolved measurements of the OPSS is given by the saturation of the third amplifier (10 V signal) and was analyzed to be about 1110 nm diameter for the current OPSS flow setup. The OPSS also counts particles larger than 1110 nm, but as these particles yield a 10 V primary signal they are not size resolved but all registered

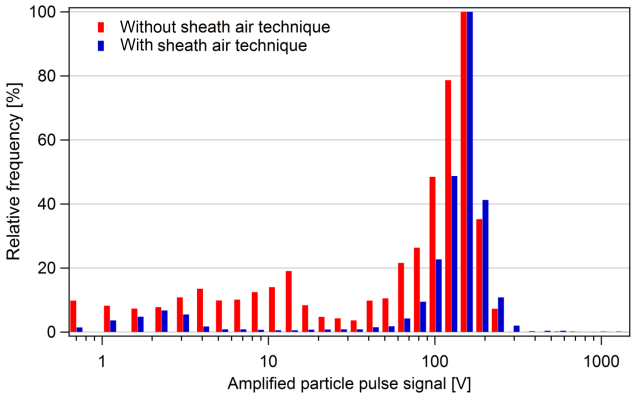

Figure 5. Signal intensity distribution measured with the CARIBIC OPSS for 350 nm PSL particle without and with implemented sheath air technique.

at the same size. Figure 4 shows two examples for a typical signal of a 200 nm and a 900 nm diameter PSL particle with a complex refractive index of $m = 1.578 - i0.0006$. The 200 nm particles cause, on average, signal pulses with a duration of about 60 µs and a maximum pulse height of 6.6 V in Ch1 (Fig. 4a). The maximum of Ch2 and Ch3 is on average 0.22 and 0.05 V, respectively. For larger particles with a diameter of, for instance, 900 nm, the amplifiers of Ch1 and Ch2 are saturated and therefore the signal is truncated at 10 V (Fig. 4b). This particle size is resolved in Ch3 with a pulse width of about 90 µs and an average pulse height of 8.65 V.

For data analysis, the signals of the three channels are combined into one quantitative signal for each particle. Therefore the signals from Ch2 and Ch3 were multiplied with a factor of 30 and 125, respectively, leading to a combined signal in the range of 0 to 1250 V. The comparison of the three amplified signals (Fig. 4c, d) shows a good agreement, which gives confidence in the amplification factors for Ch2 and Ch3. As Ch1 is the most sensitive, the signal recording of all three channels is triggered by the intensity of Ch1. The trigger level of Ch1 was set to 0.35 V for the amplified signal as for measurements of particle-free air and using a lower trigger level of 0.30 V small particle pulse signals were recorded. These artificial particle signals are caused by electronic noise. The trigger level of 0.35 V determines the lower detection limit of the OPSS, which is calculated to be about 130 nm (UT aerosol; see Sect. 3.5).

First calibrations of the modified KS-93 showed the occurrence of spurious particle signals in the size spectrum. As an example, Fig. 5 shows the output signal distribution for 350 nm PSL particles. The experimental setup (Sect. 3.1) provides a narrow, i.e., monomodal, aerosol particle number size distribution. Besides the main peak, the signal spectrum of the modified KS-93 also contained a significant number of counts, which had smaller signals, suggesting the existence of smaller particles. The additional small signals were only observed when measuring particle-loaded air but not in particle-free air. Hence the additional small signals were not caused by some kind of background noise. A potential reason for this signal intensity spread was thought to be the sampling flow geometry in the KS-93 optics. Particles passing the laser beam not in its center but instead in the edge region with reduced illumination might cause smaller particle signals. To focus the aerosol particles to the center of the laser beam, the measurement air was surrounded by particle-free sheath air in the new flow system of the CARIBIC OPSS. This sheath air is pushed through the side branch of a Swagelok tee mounted upstream of the KS93 inlet and nestled around a 0.0625 in. tubing for the sampling air located at the union center line. Using this setup four sampling-to-sheath-air ratios in the range of 1 : 3 to 1 : 15 were tested. With increasing fraction of the sheath air, the number of spurious signals decreased. However, considering that reducing the sampling air volume flow rate causes a reduction of the CARIBIC OPSS time resolution (because of sampling statistics), a sample-to-sheath-air ratio of 1 : 9 was chosen. Figure 5 shows also the distribution of the signal intensity for 350 nm PSL particles with sheath air. Clearly, the number of artifact particle signals is reduced, but it did not totally vanish. Furthermore, the 350 nm particle peak becomes narrower and its maximum is shifted to slightly larger signal intensities, both as an effect of the focusing the particles into the region with the highest laser light intensity.

The distribution of particle signals shows an increasing fraction of spurious particles and an increasing apparent particle diameter of the spurious particles with increasing real particle diameter. Using approximate relations for this behavior and six UT/LMS particle number size distributions from the literature (de Reus et al., 2000, 2001; Krejci et al., 2003; Schröder et al., 2002; Young et al., 2007; Zaizen et al., 2004), the error caused by the spurious particle pulses to the real particle number size distribution was estimated. As the UT/LMS particle number size distribution shows a steep decrease by at least 2 orders of magnitude in the size range 0.1–1.0 µm (see, e.g., Fig. 12), the error caused by the spurious particles is negligible for particles larger than 230 nm (smaller than 2 % increase in particle number concentration) and relatively small for particles below 230 nm (an increase of 2–10 %), compared to other uncertainties in the CARIBIC OPSS measurements (see Sect. 4.3).

We further investigated how to reduce this unsatisfactory feature of the CARIBIC OPSS. Looking at the particle inter-arrival times, not all inter-arrival times follow the expected exponential distribution, but some pulses show up at very short inter-arrival times. As an example, in Fig. 6 the inter-arrival times from a calibration run with 500 nm PSL particles and a number concentration of about 60 cm^{-3} are displayed. About 93 % of the particle pulses in the first two bins to the left turned out to be spurious pulses, as they cause amplified signals below 20 V, which is much lower than the 420 V for 500 nm PSL particles. Thus for UT/LMS measurements it is possible to suppress the concentration increase

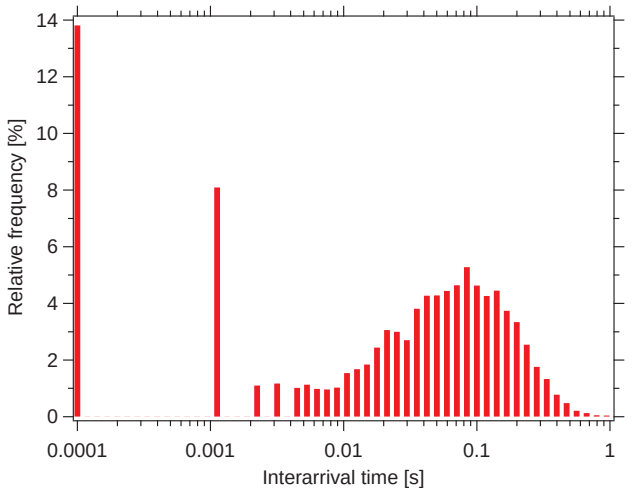

Figure 6. Inter-arrival time histogram of the CARIBIC OPSS for 500 nm PSL particles and a number concentration of about 60 particles cm^{-3}.

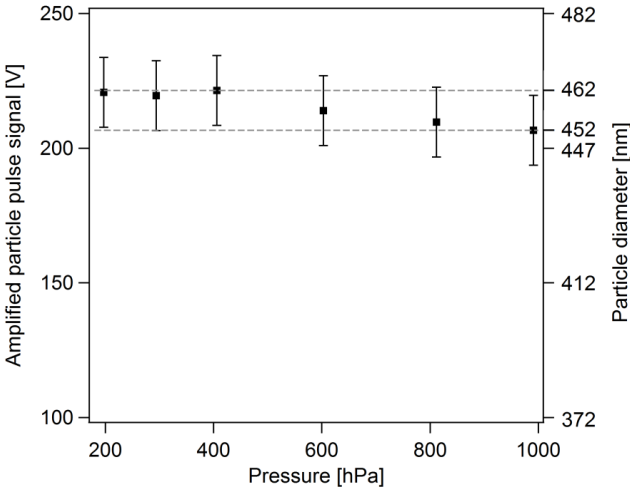

Figure 7. Particle signal pressure dependency of the CARIBIC OPSS for 450 nm PSL particles. Error bars indicate plus/minus one size bin uncertainty (out of 230 in total) in the determination of the peak distribution maximum.

caused by artificial particle pulses to a negligible level by applying an inter-arrival time filter of 0.0019 s to the measurement data, which was done for all CARIBIC flight data. However, in cases where the particle number size distribution does not fall off as steeply, like for measurements in the atmospheric boundary layer, the influence of the spurious signals cannot be neglected anymore. In this case the inter-arrival time filter does not work properly because the particle number concentration is so high that artifact and real particle pulses are not well separated anymore in the inter-arrival time diagram. For the current setup this is the case for particle number concentrations above about 200 cm^{-3} in the accumulation mode. For such an application more sophisticated criteria, like post-processing shape analysis of the pulses, might allow appropriate filtering.

3.3 Pressure dependency of the OPSS particle signal

On board the CARIBIC aircraft, the CARIBIC OPSS experiences operating pressures in the range of 250–1100 (hPa). The material of the optics (synthetic quartz cell) and the operating pressure of up to 5000 hPa specified by the manufacturer suggest no pressure dependency of the KS-93 signals. To verify this assumption the signal of 450 nm PSL particles was recorded at six pressures between 200 and 1000 hPa. For this purpose a pressure-reducing valve and a pressure sensor were installed in the calibration setup (Fig. 3) just upstream the CARIBIC OPSS. The resulting average pulse signals are displayed in Fig. 7. Although there seems to be a trend towards higher particle signals with decreasing operating pressure, this trend is only weak, with a maximum change less than 3 % in particle diameter. This uncertainty is much smaller than the uncertainty caused by the unknown refractive index of the measured atmospheric particles (15 %; see Sect. 4.3). Moreover, the experimental data almost exclusively agree within the experimental uncertainties (here defined as plus/minus one size bin (out of 230 in total) compared to the size bin with the peak maximum). Consequently there is no significant pressure dependency of the signals and thus final data are not corrected for pressure effects.

3.4 OPSS particle sizing

To determine the relation between the particle pulse height maximum and the corresponding particle diameter, the CARIBIC OPSS response function had to be determined. For this purpose calibration measurements with PSL particles were carried out and the theoretical response function was calculated for perpendicular polarized light and spherical PSL particles (refractive index of 1.578-i0.0006). The calculation of the response function is based on exact optical Mie calculation (Bohren and Huffman, 1983) in combination with a Levenberg–Marquardt algorithm for nonlinear multivariate fitting. The model considers the effects of laser polarization and spherical aperture or detection area. As free parameters the mean collecting angle, the collecting angle range, and the signal gain were used, whereas the refractive index, the polarization, and the laser wavelength were kept constant. The best fit to the PSL data points, shown in Fig. 8a, was achieved with mean collecting angle of 86.3°, a collecting angle range of ±34.8°, and a signal gain of 4016. The difference to the manufacturer values of 90° for the mean collecting angle and ±40° for the collecting angle range is caused by the nonideal behavior of the optics, the changed aerosol flow through the KS-93, and the limitations of the theory underlying the fit algorithm. With the above geometry parameters, the measured data can be reproduced very well

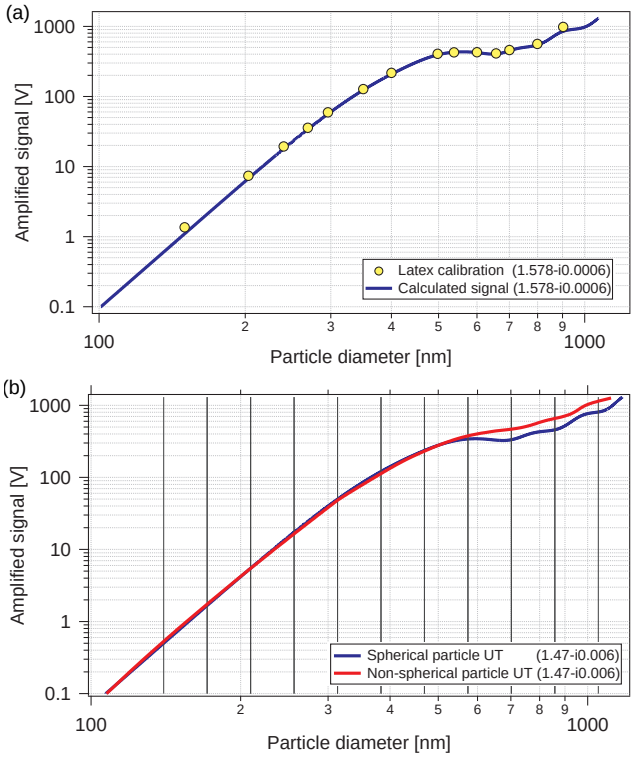

Figure 8. Response function of the CARIBIC OPSS for perpendicular polarized light: **(a)** PSL calibration measurement data and calculated PSL response function; **(b)** calculated response functions for spherical and slightly nonspherical UT particles. Solid vertical lines indicate the finally chosen particle size bin borders.

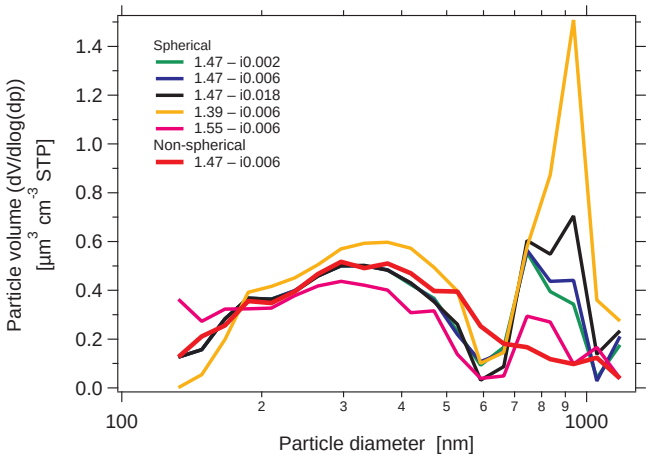

Figure 9. Particle volume distribution measured in the LMS during the CARIBIC flight LH339 on 19 April 2011 from Frankfurt, Germany, to Vancouver, Canada. Same data are displayed for six different refractive indices and using six different OPSS response functions.

and hence they were used for all other response function calculations.

The use of perpendicular polarized light in the KS-93 has the advantage of reaching a lower detection limit diameter (Bohren and Huffman, 1983) but leads to a first Mie resonance (i.e., an ambiguity in the signal-to-particle-size relation) already just above 500 nm diameter (Fig. 8a). As the polarization of the KS93 cannot be easily changed, for spherical particles the choice of size bin borders for the KS93 is therefore somewhat limited.

In order to derive the CARIBIC OPSS response function for UT/LMS particles a refractive index for these particles has to be assumed. Based on literature values (e.g., GEISA spectroscopic database at www.pole-ether.fr, accessed 1 July 2015), a uniform refractive index of 1.47-i0.006 was chosen for the CARIBIC particle number size distributions (data set version 14). This value is derived assuming an internally mixed aerosol of 45 % sulfuric acid/water, 44 % ammonium sulfate, 10 % organics, and 1 % soot for a midlatitude UT aerosol and using a volume-mixing rule for the refractive index. The choice of this refractive index is somewhat arbitrary, but not unrealistic, as the particle composition in the UT/LMS changes with altitude (Murphy et al., 2014). However, in order to have a uniform data set without discontinuities it was necessary to use only one refractive index. A sensitivity analysis on the influence of the refractive index on the derived particle size shows that the particle number size distribution would be shifted on average by 15 % in diameter towards larger diameters if, for instance, the refractive index of sulfuric acid/water (1.43-i0.001) representative for a stratospheric aerosol were used (see Sect. 4.3). With the PSL-fit-determined geometry parameters the CARIBIC OPSS response function for spherical particles and a UT/LMS refractive index of 1.47-i0.006 was calculated and is shown in Fig. 9b.

Unfortunately, the Mie resonance above 500 nm particle diameter also exists for the UT/LMS response function. Varying the refractive index in the range of 1.39 and 1.55 for the real and 0.002 and 0.018 for the imaginary part does not remove this feature. Moreover, applying the UT/LMS response function to data measured in the LMS leads to particle volume distributions not only with a first broad peak and first maximum between 250 nm and 400 nm diameter (Fig. 9) but also with a second, partly very prominent, peak above the Mie resonance. Below about 400 nm the curves for refractive indices with the same real part fall together, as expected. For this representation piecewise linear fits for the response function were used and the Mie resonance was likewise bridged with a monotonic linear section to have an unambiguous relation between the signal and the particle diameter. This last measure leads to an artificial dip in the volume distributions around 600 nm. However, the second volume peak above 700 nm is outside the Mie resonance and thus cannot be explained by this feature. This second maximum is very sensitive to the refractive index and seems to be artificial, in particular for periods of low volcanic influence on the

UT/LMS aerosol. As the particles measured by the CARIBIC OPSS are mostly dry (see Sect. 4.3), the possibility of measuring slightly nonspherical particles was considered, which would lead to a smoother response function (Pinninck et al., 1976; Borrmann et al., 2000). Therefore the UT/LMS response function was calculated again for slightly irregular-shaped particles with moderate surface structure (Pfeifer, 2014). The calculations are based on discrete dipole approximation (DDA; e.g., Yurkin and Hoekstra, 2007) and were conducted with the ADDA (absorption by discrete dipole approximation) program from Yurkin and Hoekstra (2011). The respective response function is displayed in Fig. 8b. Below 550 nm the nonspherical particle response function does not deviate strongly from the spherical particle response function, but above the Mie resonance level the difference is significant. This new response function is just one realization of many possible nonspherical response functions. However, it is a monotonic function (Fig. 8b) and leads to a smooth particle volume size distribution (Fig. 9), thus solving the problems with the spherical response function above. Hence the nonspherical response function in Fig. 8b was used for the CARIBIC OPSS UT/LMS data evaluation. There can be other reasons that lead to a similar response function (e.g., unknown properties of the optics or a particle-size-dependent refractive index); hence the use of a nonspherical particle response function is no proof that the majority of the UT/LMS particles are nonspherical.

3.5 OPSS counting efficiency

The counting efficiency of the CARIBIC OPSS, i.e., the ratio of the number of particles the CARIBIC OPSS counts to the number of available particles, is an important correction factor for the post-flight data processing. In the original setup the laser beam illuminated only half of the air sample, which limited the maximum asymptotic counting efficiency of the original KS93 to 50 %. Due to the implemented sheath air technique a higher maximum asymptotic counting efficiency could be reached. Using the calibration setup in Fig. 3 the CARIBIC OPSS counting efficiency was determined for PSL and AS particles with the CPC as reference instrument. Because of existing water peaks, with particle diameters below 100 nm, which would be counted by the CPC but not by the CARIBIC OPSS, only DMA selected particles were used for determining the OPSS counting efficiency. For our setup the counting efficiency $\varepsilon(d_\mathrm{p})$ is defined as

$$\varepsilon(d_\mathrm{p}) = \frac{N_\mathrm{OPSS}}{N_\mathrm{CPC}}, \tag{1}$$

with N as the particle number concentration measured at a given particle diameter, d_p. When using monodisperse PSL particles, the measured particle number concentrations (corrected for the spurious signals at smaller particle diameters; see Sect. 3.2) can be directly compared for each particle size. The four measurement points with PSL standards 125, 200, 350, and 500 nm were complemented with AS particles. These multiply charged AS particles (as result of the DMA) were resolved in size by using 256 size bins for the CARIBIC OPSS data analysis. Using these highly resolved data the counting efficiency of the CARIBIC OPSS was calculated iteratively from large particle sizes to smaller ones. For each singlet maximum diameter the number of all multiple charged particles (N_multiple) measured by the OPSS was summed for all larger size bins i (Eq. 2).

$$N_\mathrm{multiple} = \sum_i \frac{N_i}{\varepsilon_i} \tag{2}$$

Therefore the counting efficiency for the doublets, triplets, and larger particle sizes was taken into account. The respective counting efficiencies were taken from the previous calibration steps. For the first calibration step (largest particles, 500 nm AS), the particle generator was operated with a salt concentration low enough to guarantee that multiply charged particles were not present; hence N_multiple was 0.

By subtracting N_multiple from the number of particles the CPC counted (N_CPC), the total number of singly charged particles was calculated ($N_\mathrm{CPC,s}$; Eq. 3). Dividing the number of singly charged particles the CARIBIC OPSS counted ($N_\mathrm{OPSS,s}$; Eq. 4, with a and b the size bin borders of the singly charged particle peak) by $N_\mathrm{CPC,s}$, the OPSS counting efficiency $\varepsilon(d_\mathrm{p})$ at the particle diameter of the singlets was finally determined (Eq. 5).

$$N_\mathrm{CPC,s} = N_\mathrm{CPC} - N_\mathrm{multiple} \tag{3}$$

$$N_\mathrm{OPSS,s} = \sum_{i=a}^{b} N_i \tag{4}$$

$$\varepsilon(d_\mathrm{p}) = \frac{N_\mathrm{OPSS,s}}{N_\mathrm{CPC,s}} \tag{5}$$

The resulting counting efficiency curve is displayed in Fig. 10. Like for the size calibration, all particle diameters were related to an UT aerosol. Above about 200 nm, the OPSS counting efficiency is constant and reaches a maximum asymptotic counting efficiency of 98 %. For smaller particle diameters the counting efficiency decreases. The particle diameter where the counting efficiency is half the maximum asymptotic counting efficiency ($d_{\mathrm{p}_{50}}$) characterizes the lower detection limit of a particle counter. Using Eq. (6) as fitting function (Wiedensohler et al., 1997), the CARIBIC OPSS $d_{\mathrm{p}_{50}}$ for a midlatitude UT aerosol was calculated as 152 nm.

$$\varepsilon(d_\mathrm{p}) = A - \frac{B}{1 + \exp\left(\frac{d_\mathrm{p} - d_{\mathrm{p}_1}}{d_{\mathrm{p}_2}}\right)} \tag{6}$$

3.6 OPSS particle coincidence

Although particle coincidence is in general a minor problem for measurements methods using a sheath air technique,

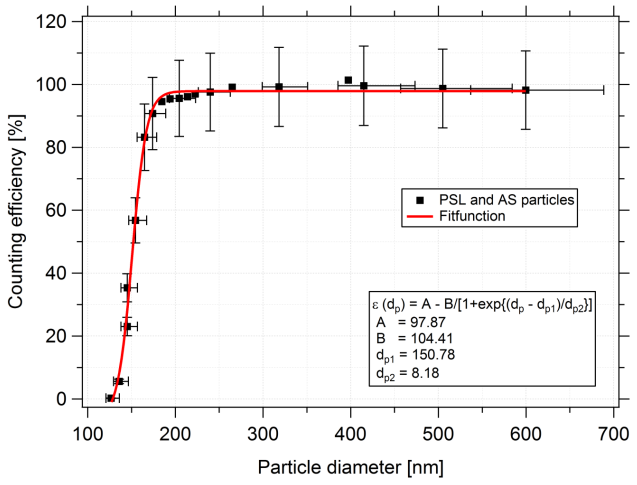

Figure 10. Counting efficiency of the CARIBIC OPSS for UT particles (refractive index of 1.47-i0.006).

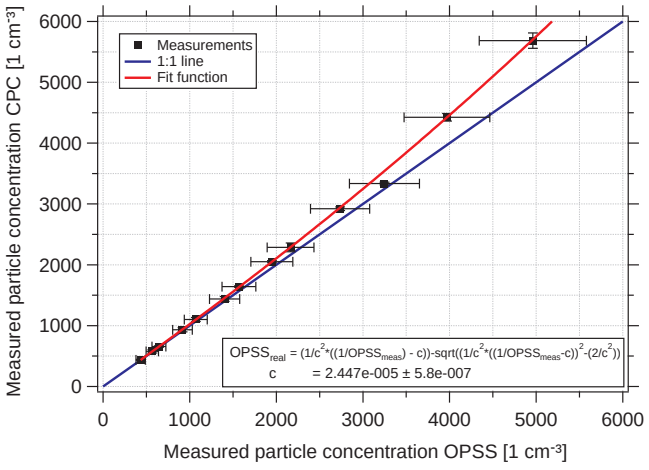

Figure 11. Particle coincidence in the CARIBIC OPSS measured for 200 nm PSL particles.

the effect of two particles being in the optical field of view at the same time was investigated for the CARIBIC OPSS. For that purpose the number concentrations measured by the CARIBIC OPSS for 200 nm PSL particles and corrected for the counting efficiency (Sect. 3.5) were compared to the number concentrations measured by the CPC, corrected for coincidence. Figure 11 shows the respective results. The coincidence effect is below 4 % for an ambient particle number concentration of 1500 cm^{-3}. Considering that, based on CARIBIC measurements, the ambient accumulation mode particle number concentration in the UT/LMS rarely exceeds 100 cm^{-3} (coincidence below 0.25 %), the raw data were not corrected for coincidence in the post-flight data processing.

4 Data evaluation

4.1 Post-flight data processing

For post-flight analysis of the CARIBIC OPSS data a FORTRAN program was written that converts the raw data into a particle number size distribution. The program first converts the amplified raw signal maxima of a particle pulse to a particle size using the size calibration curve (Sect. 3.4 and Fig. 8). The obtained particle sizes are then sorted into a histogram with logarithmically equidistant size bins. For the current data version (V14), the resolution was set to 10 size bins and an averaging time of 180 s. As the uncertainty of the counting efficiency at particle diameters well below the $d_{p_{50}}$ leads to particle number concentration uncertainties of several tens of percent, the CARIBIC particle size distributions do not include data below 140 nm particle diameter. Due to the saturation of the signal amplifiers and in order to be able to clearly resolve at least the maximum of each particle signal, the CARIBIC particle size distributions were limited to 1050 nm on the upper end of the size distribution.

To obtain the particle number size distribution, i.e., the number concentration for each size bin, the program calculates the volume flow through the CARIBIC OPSS from the MFC-derived mass flows and the measured air temperature and pressure. All concentrations are converted from ambient to standard atmospheric conditions ($T = 273.15$ K, $p = 1013.25$ hPa). The program also corrects the data for the counting efficiency of the CARIBIC OPSS (Sect. 3.5) and for particle losses in the inlet and the sampling line between the inlet tip and the CARIBIC OPSS (3±1 %; Weigelt, 2015). These sampling losses are estimated based on empirical equations from the literature and wind tunnel experiments with another aircraft-borne aerosol inlet (Hermann et al., 2001). Particle coincidence can be neglected for the UT/LMS (see Sect. 3.6). In addition to the particle number size distribution, concentrations of the integral particle number, the particle surface area, the particle volume, the particle mass (assuming a particle density of 1.66 g cm^{-3} based on the same composition used for calculating the refractive index above), as well as the geometric mean particle diameter are calculated. Moreover, the particle surface, volume, and mass distributions can be calculated.

When analyzing the first flight data it was found that high, short-time peaks in the CARIBIC OPSS particle number and mass concentrations correlated well with the occurrence of clouds (Martinsson et al., 2014; Weigelt, 2015). The latter were identified using the cloud water content measured in parallel in situ by the CARIBIC water instruments (Dyroff et al., 2014) and, when this parameter was not available, using the modeled cloud water content from KNMI (www.knmi.nl/samenw/campaign_support/CARIBIC/index.html, accessed 1 July 2015). Following the Kelvin–Köhler theory, the interstitial accumulation mode particle number inside clouds should be lowered due to the activation of these particles to cloud droplets. However, the CARIBIC OPSS particle

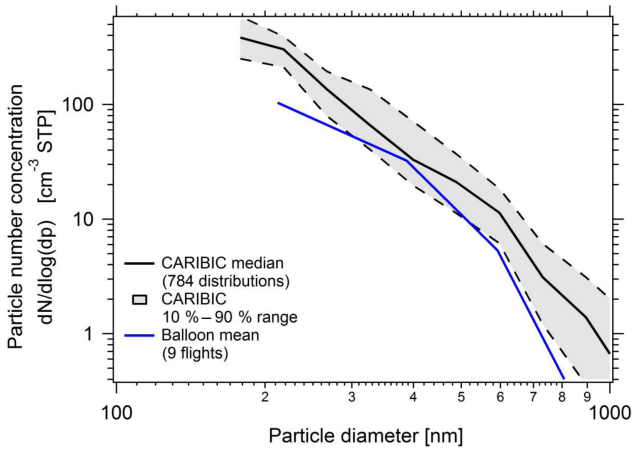

Figure 12. Comparison of particle number size distributions measured with a balloon-borne OPSS (Deshler et al., 2003) and the CARIBIC OPSS. Underlying data were all taken in the midlatitude LMS (south of 65° N; 150–700 ppbv ozone) from periods in 2010–2013 with little or no volcanic influence on the LMS aerosol (see Andersson et al., 2015, Fig. 1).

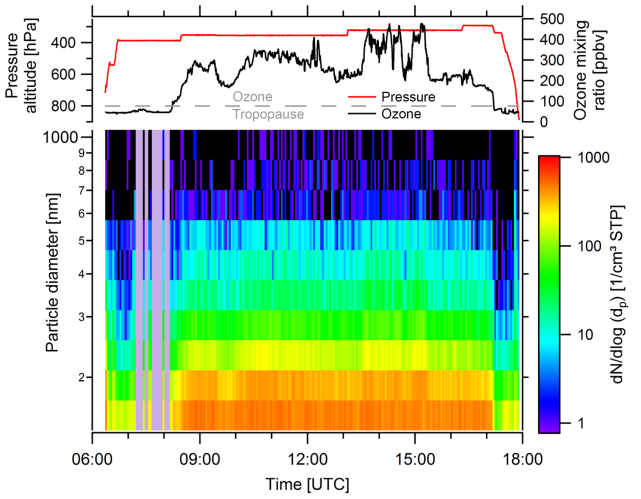

Figure 13. Accumulation mode particle number size distribution for the CARIBIC flight LH454 from Seoul, South Korea, to Frankfurt, Germany, on 4 December 2013. Cruise level data are obtained almost exclusively in the LMS, in air masses which are characteristic for air from 2 to 3 km above the thermal tropopause (see www.knmi.nl/samenw/campaign_support/CARIBIC/041213a/index.html, accessed 1 July 2015). The red line gives the aircraft pressure altitude, the black line the ozone mixing ratio, and the color code the particle number concentration in 10 particle size bins. Gray bars indicate periods of inside cloud measurements.

number size distributions showed for all particle diameters equal or higher particle number concentrations inside clouds compared to outside. Therefore it must be assumed that the CARIBIC OPSS inside cloud measurements are biased by particle artifacts caused by cloud droplet breakup at the inlet tip (Korolev et al., 2011, 2013). Consequently, all in-cloud data were flagged as "missing data" in the CARIBIC OPSS data set. These cloud-influenced data fractions amount to 0.6 to 20 % of the OPSS measurements at cruise altitude, depending on the atmospheric region (i.e., LMS or UT).

4.2 Comparison with balloon-borne measurements

To evaluate the resulting data we compared the particle number size distributions measured by the CARIBIC OPSS with balloon-borne in situ measurements over Laramie, Wyoming, USA (Deshler et al., 2003). For the comparison two periods of little volcanic influence (according to Andersson et al., 2015) were chosen, from June 2010 to May 2011 and from May 2012 to June 2013. Data from these periods are considered representative for the background aerosol. The balloon and CARIBIC particle size distribution data sets in these two periods were restricted to measurements between 30 and 65° N and to the LMS (ozone values between 150 and 700 ppbv), as the LMS aerosol shows much less variation with sampling location than the UT aerosol (see Fig. 13). Thus the large spatial distance between Laramie, Wyoming, and the CARIBIC data sampling location has little influence on the comparison. The resulting size distributions are shown in Fig. 12. In order to account for the evaporation of water and thus the shrinking of the aerosol particles during transport through the CARIBIC inlet system (see Sect. 4.3), the CARIBIC size distribution was shifted by 15 % in diameter towards larger particle diameters. Consequently all curves represent ambient distributions. The balloon mean and the CARIBIC OPSS median number size distributions look quite similar in shape and magnitude. However, the balloon number size distribution agrees best with the CARIBIC OPSS 10 % percentile number size distribution, which is about a factor of 2 lower in concentration than the CARIBIC OPSS median number size distribution. A clear reason for this factor of 2 cannot be given yet, as both instruments are well characterized. The difference in the used refractive indices, i.e., 1.45-i.0.0 (balloon) and 1.47-i0.006 (CARIBIC), cannot account for this factor of 2 because adapting to the balloon data refractive index would shift the CARIBIC particle diameters only by 1–3 %, and this, moreover, mostly towards larger particle diameters. One reason might be that there is still some variability in the LMS aerosol with longitude (both in number and in refractive index) and thus the different sampling locations could contribute to the observed difference. Another reason might be connected to the measurement platform, as one of the two instruments was mounted on board a jet aircraft whereas the other was ascending on a balloon. However, a comparison between aircraft-borne particle number size distribution measurements given in the literature (de Reus et al., 2000, 2001; Krejci et al., 2003; Schröder et al., 2002; Young et al., 2007; Zaizen et al., 2004) yielded an even higher scatter among the individual data sets (Weigelt, 2015).

4.3 Measurement uncertainties

Concerning the measured particle number size distributions, three kinds of uncertainties have to be considered: the statistical counting uncertainty, the instrumental uncertainty with respect to particle number concentration, and the instrumental uncertainty with respect to particle sizing.

The statistical uncertainty of the particle number concentration measurements arises due to the fact that particle counting follows the Poisson statistics (e.g., Fukutsu et al., 1999; Damit et al., 2014). Consequently the standard deviation σ_N due to counting uncertainty of a measured total accumulation mode particle number concentration N_{140} is given (in percent) by

$$\sigma_N = \frac{\sqrt{N_{140}}}{N_{140}} \times 100 = \frac{100}{\sqrt{N_{140}}}. \quad (7)$$

The CARIBIC OPSS uncertainty with respect to particle number concentrations is caused by the uncertainties of the OPSS flow rate (14 %, MFC uncertainties) and the OPSS counting efficiency (5 % for diameters larger than 200 nm, measurement uncertainty). An additional uncertainty of 15 % for the individual size bin particle number concentration is caused by the particle refractive index, as different response functions can attribute a given particle signal into different size bins. The above uncertainty was calculated using fixed OPSS size bins, real CARIBIC flight data, and three different response functions. Finally the inlet sampling efficiency for accumulation mode particles contributes to the OPSS number concentration uncertainty with about 10 %. This number was estimated from the standard deviation of the wind tunnel experiment particle transmission data of the inlet. To these randomly distributed uncertainties (Gaussian error propagation) the error caused by the spurious particle signals (below 1 %) must be added, whereas coincidence again can be neglected. This error propagation yields a total instrumental uncertainty with respect to the particle number concentration of 19 % for the total accumulation mode particle number and 25 % for the individual size bins.

The uncertainty of the CARIBIC OPSS with respect to particle size is determined by four factors: the uncertainty of the size calibration, the use of a single complex refractive index for all particles, the particle shape, and the evaporation of particle material during transport through the sampling line. The uncertainty of the size calibration can be estimated using the width of the Gaussian signal distribution when measuring a quasi-monodisperse aerosol. According to laboratory calibrations this uncertainty is 6 % for the CARIBIC OPSS (Weigelt, 2015). As the particles used for the calibration are only quasi-monodisperse, their size distribution width already causes some of the spread in the OPSS data, and thus this number is an upper limit.

Uncertainties caused by the unknown refractive index of atmospheric particles were estimated for one measurement flight by three refractive indices representative for the mid-latitude upper troposphere, the lowermost stratosphere, and the tropical middle troposphere (Weigelt, 2015). For these calculations the 10 h CARIBIC flight LH317 from Frankfurt/Germany to Johannesburg/South Africa on 15 November 2010 was chosen because it passed all three atmospheric regions. According to this estimate the uncertainty in the OPSS-derived particle size is about 15 % in particle diameter and nearly independent of particle size. This value is derived from the size distributions with the two refractive indices, which yielded the most differing size distribution curves.

The particle size uncertainty caused by the unknown particle shape is hard to estimate. Ideally, one would take different original OPSS particle signals, use dozens of different OPSS response functions, each derived for a different particle shape, to transfer the signals into particle sizes, and finally calculate for each original particle signal a particle size probability function. This huge effort could not be carried out in this study. The discussion about the OPSS response function in Sect. 3.4 and the volume distribution in Fig. 9 already indicates, however, that the particle size uncertainty caused by the unknown particle shape is not small for particles in the size range of the laser wavelength or above.

Finally, the evaporation of particle material during transport from the inlet system to the CARIBIC OPSS leads to an uncertainty concerning the determined particle size. As the measurement air is heated from about $-55\,^{\circ}\mathrm{C}$ in the ambient UT/LMS to about $+25\,^{\circ}\mathrm{C}$ in the measurement container, the measured particles can be assumed to be mostly dry. Box model calculations for the evaporation of stratospheric sulfuric acid/water particles in the CARIBIC sampling line indicated that for accumulation mode particles about 84–88 % of the water is evaporated (depending on particle size) when the particles reach the OPSS whereas sulfuric acid remains almost completely particle bound (1–8 % losses). As the changes in particle size due to the leftover water and the evaporated sulfuric acid partly cancel each other out the measured particle diameter agrees within 5 % with the ambient dry particle diameter. As the real particle composition in the UT is different from pure sulfuric acid/water (Murphy et al., 2014) and in particular the fraction, composition, and properties of the organic particle material is not known yet, it is hard to calculate the respective shrinking of UT particles.

5 CARIBIC OPSS application

Since June 2010, the OPSS is part of the CARIBIC measurement container on board a Lufthansa Airbus A340-600 (www.caribic-atmospheric.com, Brenninkmeijer et al., 2007). In CARIBIC, two to four intercontinental flights per month are carried out with this flying laboratory, as one of the two pillars of IAGOS. Particle size distributions measured during two of these flights are displayed in Figs. 13 and 14. Figure 13 shows the particle number size distribution for the CARIBIC flight LH454 from Seoul, South Korea, to Frank-

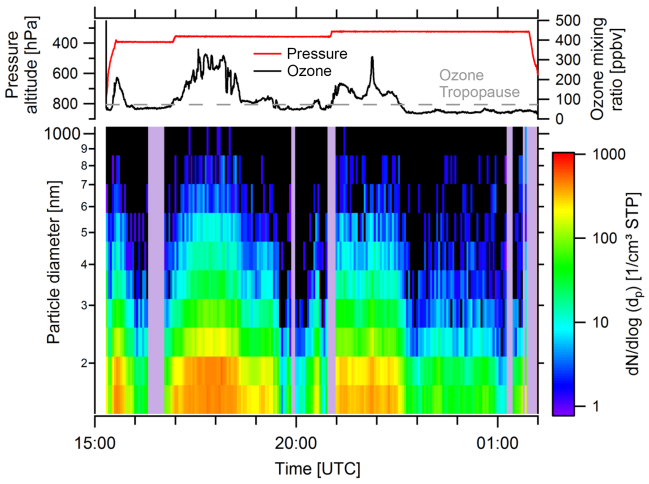

Figure 14. Accumulation mode particle number size distribution for the CARIBIC flight LH319 from Frankfurt, Germany, to Bogota, Columbia, on 16 November 2010. This flight is characterized by alternating tropospheric and stratospheric flight sections (see ozone mixing ratio and www.knmi.nl/samenw/campaign_support/CARIBIC/161110/index.html, accessed 1 July 2015). Same representation as in Fig. 13.

furt, Germany, on 4 December 2013. Almost all cruise altitude data (10.6–12.2 km) were taken in the LMS (see ozone mixing ratio). Of these LMS measurements, 86 % were in air masses, which are characteristic for air 2 to 3 km above the thermal tropopause. As passenger aircraft fly in a narrow cruise altitude range (about 9–12 km), the large distance to the local tropopause can only be reached by the displacement of the local tropopause relative to the aircraft, for instance in a tropopause fold. The particle number size distribution in the LMS shows little variation with the sampling region (the time axis in Fig. 13 is virtually a longitude axis because of the mainly east–west flight track), with a standard deviation of only 9 and 17 % in total accumulation mode particle number and mass concentration, respectively. This variation is moreover mainly caused by changes in the flight altitude, as there are strong vertical gradients in aerosol concentrations in the tropopause region (e.g., Brock et al., 1995; Martinsson et al., 2005).

Figure 14 displays the accumulation mode particle number size distribution for the CARIBIC flight LH319 from Frankfurt, Germany, to Bogota, Columbia, on 16 November 2010, measured at cruise altitudes of 10.4–11.6 km. Three times the aircraft changed between tropospheric and stratospheric flight sections, which can be clearly seen not only in the ozone mixing ratio but also by the aerosol color pattern in Fig. 14. Midlatitude tropospheric sections show on average a factor of about 10 lower accumulation mode particle concentrations (both in number and mass) compared to the stratospheric sections. This concentration difference is caused by the continuous supply of particle mass from the middle and upper stratosphere with the Brewer–Dobson circulation (Deshler, 2008) and the scavenging of accumulation mode particles by clouds in the troposphere (e.g., Ekman et al., 2006).

6 Conclusions

A new optical particle size spectrometer for aircraft-borne measurements of the particle number size distribution between 140 and 1050 nm diameter in the upper troposphere and lowermost stratosphere is presented in this study. The core instrument, a commercial RION KS-93 particle sensor, was modified to record individual particle pulse signal curves together with a time stamp. Due to this high-resolution sampling, the OPSS particle size bin width and the OPSS size distribution time resolution can be adapted at any time after measurement. Moreover, additional filtering by inter-arrival time, pulse width, and maybe even pulse area could be carried out in the future. Because of the robust synthetic quartz optics, the particle signals show no pressure dependency in the operating pressure range of 200–1000 hPa. Installed into a 19 in. EMC rack unit the modified KS-93, the data acquisition, and the new airflow system compose the new OPSS. The particle counting efficiency of the OPSS could be increased from originally 50 to 98 % by using a sheath air technique, as shown by polystyrene latex and ammonium sulfate particle calibration measurements. The sheath air reduced the probability of particle coincidence to less than 4 % for an ambient particle number concentration of 1500 cm^{-3}. The occurrence of spurious particle pulses was suppressed below 1 % due to the sheath air and the application of an inter-arrival time filter on the data. The latter, however, works only for low ambient particle number concentrations of about 200 cm^{-3} or less in the accumulation mode, as for instance encountered in the free troposphere and lowermost stratosphere. The size response function of the OPSS, which connects the measured scattered light signal to the particle diameter, was derived from polystyrene latex calibration measurements and model calculations for spherical and slightly nonspherical particles. The nonspherical particle response function was finally chosen for data evaluation, as it leads to smoother particle volume distributions. The use of a nonspherical particle response function is no proof that the majority of the UT/LMS particles are nonspherical. There can be other reasons which lead to a similar response function, for instance unknown properties of the optics or a particle-size-dependent refractive index. A comparison with LMS particle number size distributions measured from balloons (Deshler et al., 2003) yielded an agreement within a factor of 2 in number concentration.

Since June 2010 the new OPSS is regularly flown once per month for four intercontinental flights inside the CARIBIC measurement container on board a Lufthansa Airbus (Brenninkmeijer et al., 2007). Since then, the CARIBIC OPSS has

measured accumulation mode particle number size distributions on more than 1 million flight km, mainly in the northern hemispheric UT/LMS (see www.caribic-atmospheric.com/2005/Flight_Scheduling.html, accessed 1 July 2015). Besides information about UT/LMS aerosol particle transport, transformation, lifetime, and trends, these measurements provide a unique data set for the validation of remote sensing instruments or global atmospheric aerosol models.

Acknowledgements. We thank Lufthansa and Lufthansa Technik for enabling CARIBIC and the logistical support. Without their willingness to support this for a commercial airline unusual project, CARIBIC would not exist. The German Research Foundation (DFG) is acknowledged for their financial support of the data analysis within the Priority Programme 1294 (HALO). Moreover, the German Federal Ministry of Education and Research (BMBF) is acknowledged for financing the instruments operation as part of the joint project IAGOS-D. The balloon-borne measurements above Laramie, Wyoming, were supported by the US National Science Foundation. Finally, we thank M. Werner (TROPOS) for his help with the CARIBIC OPSS electronics and P. van Velthoven (KNMI) for providing meteorological data.

Edited by: S. Malinowski

References

Andersson, S. M., Martinsson, B. G., Vernier, J. P., Friberg, J., Brenninkmeijer, C. A. M., Hermann, M., van Velthoven, P. F. J., and Zahn, A., Significant radiative impact of volcanic aerosol in the lowermost stratosphere, Nat. Commun., 6, 7692, doi:10.1038/ncomms8692, 2015.

Bohren, C. F. and Huffman, D. R.: Absorption and scattering of light by small particles, John Wiley & Sons, New York, 530 pp., 1983.

Borrmann, S., Luo, B., and Mishchenko, M.: Application of the T-Matrix method to the measurement of aspherical (ellipsoidal) particles with forward scattering optical particle counters, J. Aerosol Sci., 31, 789–799, doi:10.1016/S0021-8502(99)00563-7, 2000.

Brenninkmeijer, C. A. M., Crutzen, P., Boumard, F., Dauer, T., Dix, B., Ebinghaus, R., Filippi, D., Fischer, H., Franke, H., Frieß, U., Heintzenberg, J., Helleis, F., Hermann, M., Kock, H. H., Koeppel, C., Lelieveld, J., Leuenberger, M., Martinsson, B. G., Miemczyk, S., Moret, H. P., Nguyen, H. N., Nyfeler, P., Oram, D., O'Sullivan, D., Penkett, S., Platt, U., Pupek, M., Ramonet, M., Randa, B., Reichelt, M., Rhee, T. S., Rohwer, J., Rosenfeld, K., Scharffe, D., Schlager, H., Schumann, U., Slemr, F., Sprung, D., Stock, P., Thaler, R., Valentino, F., van Velthoven, P., Waibel, A., Wandel, A., Waschitschek, K., Wiedensohler, A., Xueref-Remy, I., Zahn, A., Zech, U., and Ziereis, H.: Civil Aircraft for the regular investigation of the atmosphere based on an instrumented container: The new CARIBIC system, Atmos. Chem. Phys., 7, 4953–4976, doi:10.5194/acp-7-4953-2007, 2007.

Brock, C. A., Hamill, P., Wilson, J. C., Jonsson, H. H., and Chan, K. R.: Particle formation in the upper tropical troposphere: A source of nuclei for the stratospheric aerosol, Science, 270, 1650–1653, doi:10.1126/science.270.5242.1650, 1995.

Cai, Y., Snider, J. R., and Wechsler, P.: Calibration of the passive cavity aerosol spectrometer probe for airborne determination of the size distribution, Atmos. Meas. Tech., 6, 2349–2358, doi:10.5194/amt-6-2349-2013, 2013.

Charlson, R. J., Schwartz, S. E., Hales, J. M., Cess, R. D., Coakley Jr., J. A., Hansen, J. E., and Hofmann, D. J., Climate forcing by anthropogenic aerosols, Science, 255, 423–430, doi:10.1126/science.255.5043.423, 1992.

Damit, B., Wu, C.-Y., and Cheng, M.-D.: On the Validity of the Poisson Assumption in Sampling Nanometer-Sized Aerosols, Aerosol Sci. Technol., 48, 562–570, doi:10.1080/02786826.2014.899682, 2014.

de Reus, M., Ström, J., Curtius, J., Pirjola, Vignati, E., Arnold, F., Hansson, H. C., Kulmala, M., Lelivield, J., and Raes, F.: Aerosol production and growth in the upper free troposphere, J. Geophys. Res. 105, 24751–24762, doi:10.1029/2000JD900382, 2000.

de Reus, M., Krejci, R. Williams, J., Fischer, H., Scheele, R., and Ström, J.: Vertical and horizontal distributions of the aerosol number concentration and size distribution over the northern Indian Ocean, J. Geophys. Res., 106, 28629–28641, doi:10.1029/2001JD900017, 2001.

Deshler, T.: A review of global stratospheric aerosol: Measurements, importance, life cycle, and local stratospheric aerosol, Atmos. Res., 90, 223–232, doi:10.1016/j.atmosres.2008.03.016, 2008.

Deshler, T., Hervig, M. E., Hofmann, D. J., Rosen, J. M., and Liley, J.: Thirty years of in situ stratospheric aerosol size distribution measurements from Laramie, Wyoming (41° N), using balloon-borne instruments, J. Geophys. Res., 108, 4167, doi:10.1029/2002JD002514, 2003.

Dyroff, Ch., Zahn, A., Christner, E., Forbes, R., Tompkins, A. M., and van Velthoven, P. F. J.: Comparison of ECMWF analysis and forecast humidity data to CARIBIC upper troposphere and lower stratosphere observations, Q. J. Roy. Meteor. Soc., 141, 833–844, doi:10.1002/qj.2400, 2014.

Ekman, A. M. L., Wang, C., Ström, J., and Krejci, R.: Explicit simulation of aerosol physics in a cloud-resolving model: aerosol transport and processing in the free troposphere, J. Atmos. Sci., 63, 682–696, doi:10.1175/JAS3645.1, 2006.

Fukutsu, K., Yamada, Y., Koizumi, A., and Shimo, M.: A statistical study on the design of particle count measurements, J. Aerosol Res. Jpn., 4, 55–62, doi:10.11203/jar.14.55, 1999.

Gebhart, J.: Optical direct-reading techniques: light intensity systems, in: Aerosol Measurement: Principles, Techniques, and Applications, edited by: Baron, P. A. and Willeke, K., Wiley-Interscience, New York, USA, 419–454, 2001.

Hermann, M. and Wiedensohler, A.: Counting efficiency of condensation particle counters at low-pressures with illustrative data from the upper troposphere, J. Aerosol Sci., 32, 975–991, 2001.

Hermann, M., Stratmann, F., Wilck, M., and Wiedensohler, A.: Sampling characteristics of an aircraft-borne aerosol inlet system, J. Atmos. Ocean. Tech. 18, 7–19, doi:10.1175/1520-0426(2001)018<0007:scoaab>2.0.co;2, 2001.

Korolev, A. V., Emery, E. E., Strapp, J. W., Cober, S. G., Isaac, G. A., Wasey, M., and Marcotte, D.: Small ice particles in tropospheric clouds: fact or artifact?, B. Am. Meteorol. Soc., 91, 967–973, doi:10.1175/2010BAMS3141.1, 2011.

Korolev, A. V., Emery, E. F., Strapp, J. W., Cober, S. G., and Isaac, G. A.: Quantification of the effects of shattering on airborne ice particle measurements, J. Atmos. Ocean. Tech., 30, 2527–2553, doi:10.1175/JTECH-D-13-00115.1, 2013.

Krämer, M., Schiller, C., Afchine, A., Bauer, R., Gensch, I., Mangold, A., Schlicht, S., Spelten, N., Sitnikov, N., Borrmann, S., de Reus, M., and Spichtinger, P.: Ice supersaturations and cirrus cloud crystal numbers, Atmos. Chem. Phys., 9, 3505–3522, doi:10.5194/acp-9-3505-2009, 2009.

Krejci, R., Ström, J., de Reus, M., Hoor, P., Williams, J., Fischer, H., and Hansson, H.-C.: Evolution of aerosol properties over the rain forest in Surinam, South America, observed from aircraft during the LBA-CLAIRE 98 experiment, J. Geophys. Res., 108, 4561, doi:10.1029/2001JD001375, 2003.

Mann, G. W., Carslaw, K. S., Reddington, C. L., Pringle, K. J., Schulz, M., Asmi, A., Spracklen, D. V., Ridley, D. A., Woodhouse, M. T., Lee, L. A., Zhang, K., Ghan, S. J., Easter, R. C., Liu, X., Stier, P., Lee, Y. H., Adams, P. J., Tost, H., Lelieveld, J., Bauer, S. E., Tsigaridis, K., van Noije, T. P. C., Strunk, A., Vignati, E., Bellouin, N., Dalvi, M., Johnson, C. E., Bergman, T., Kokkola, H., von Salzen, K., Yu, F., Luo, G., Petzold, A., Heintzenberg, J., Clarke, A., Ogren, J. A., Gras, J., Baltensperger, U., Kaminski, U., Jennings, S. G., O'Dowd, C. D., Harrison, R. M., Beddows, D. C. S., Kulmala, M., Viisanen, Y., Ulevicius, V., Mihalopoulos, N., Zdimal, V., Fiebig, M., Hansson, H.-C., Swietlicki, E., and Henzing, J. S.: Intercomparison and evaluation of global aerosol microphysical properties among AeroCom models of a range of complexity, Atmos. Chem. Phys., 14, 4679–4713, doi:10.5194/acp-14-4679-2014, 2014.

Martinsson, B. G., Nguyen, H. N., Brenninkmeijer, C. A. M., Zahn, A., Heintzenberg, J., Hermann, M., and van Velthoven, P. F. J.: Characteristics and origin of lowermost stratospheric aerosol at northern midlatitudes under volcanically quiescent conditions based on CARIBIC observations, J. Geophys. Res., 110, D12201, doi:10.1029/2004JD005644, 2005.

Martinsson, B. G., Friberg, J., Andersson, S. M., Weigelt, A., Hermann, M., Assmann, D., Voigtländer, J., Brenninkmeijer, C. A. M., van Velthoven, P. J. F., and Zahn, A.: Comparison between CARIBIC Aerosol Samples Analysed by Accelerator-Based Methods and Optical Particle Counter Measurements, Atmos. Meas. Tech., 7, 2581–2596, doi:10.5194/amt-7-2581-2014, 2014.

Murphy, D. M., Froyd, K. D., Schwarz, J. P., and Wilson, J. C.: Observations of the chemical composition of stratospheric aerosol particles, Q. J. Roy. Meteor. Soc., 140, 1269–1278, doi:10.1002/qj.2213, 2014.

Nguyen, H. N., Gudmundsson, A., and Martinsson, B. G.: Design and calibration of a multi-channel aerosol sampler for studies of the tropopause region from the CARIBIC platform, Aerosol Sci. Tech., 40, 649–655, 2006.

Pfeifer, S.: Verknüpfung aerodynamischer und optischer Eigenschaften nichtkugelförmiger atmosphärischer Grobstaubpartikel, PhD Thesis, University Leipzig, Dresden, Germany, available at: http://www.qucosa.de/recherche/frontdoor/cache.off?tx_slubopus4frontend[id]=15856 (last access: 3 November 2015), 2014.

Pinnick, R. G., Carroll, D. E., and Hoffmann, D. J.: Polarized light scattered from monodisperse randomly oriented nonspherical aerosol particles: measurements, Appl. Optics, 15, 384–393, 1976.

Rauthe-Schöch, A., Weigelt, A., Hermann, M., Martinsson, B. G., Baker, A. K., Heue, K.-P., Brenninkmeijer, C. A. M., Zahn, A., Scharffe, D., Eckhardt, S., Stohl, A., and van Velthoven, P. F. J.: CARIBIC aircraft measurements of Eyjafjallajökull volcanic clouds in April/May 2010, Atmos. Chem. Phys., 12, 879–902, doi:10.5194/acp-12-879-2012, 2012.

Rosenberg, P. D., Dean, A. R., Williams, P. I., Dorsey, J. R., Minikin, A., Pickering, M. A., and Petzold, A.: Particle sizing calibration with refractive index correction for light scattering optical particle counters and impacts upon PCASP and CDP data collected during the Fennec campaign, Atmos. Meas. Tech., 5, 1147–1163, doi:10.5194/amt-5-1147-2012, 2012.

Schröder, F., Kärcher, B., Fiebig, M., and Petzold, A.: Aerosol states in the free troposphere at northern midlatitudes, J. Geophys. Res., 107, 8126, doi:10.1029/2000JD000194, 2002.

Seinfeld, J. H. and Pandis, S. N.: Atmospheric Chemistry and Physics: from Air Pollution to Climate Change, 1st Edn., J. Wiley, New York, USA, 1326 pp., 1998.

Søvde, O. A., Gauss, M., Isaksen, I. S. A., Pitari, G., and Marizy, C.: Aircraft pollution – a futuristic view, Atmos. Chem. Phys., 7, 3621–3632, doi:10.5194/acp-7-3621-2007, 2007.

Vernier, J.-P., Thomason, L. W., and Kar, J.: CALIPSO detection of an Asian tropopause aerosol layer, Geophys. Res. Lett., 38, L07804, doi:10.1029/2010GL046614, 2011.

Weigelt, A.: An optical particle counter for the regular application onboard a passenger aircraft: instrument modification, characterization and results from the first year of operation, PhD thesis, Universität Leipzig, Leipzig, 204 pp., 2015.

Wiedensohler, A., Orsini, D., Covert, D. S., Coffmann, D., Cantrell, W., Havlicek, M., Brechtel, F. J., Russell, L. M., Weber, R. J., Gras, J., Hudson, J. G., and Litchy, M.: Intercomparison study of size-dependent counting efficiency of 26 condensation particle counters, Aerosol Sci. Tech., 27, 224–242, 1997.

Wiedensohler, A., Birmili, W., Nowak, A., Sonntag, A., Weinhold, K., Merkel, M., Wehner, B., Tuch, T., Pfeifer, S., Fiebig, M., Fjäraa, A. M., Asmi, E., Sellegri, K., Depuy, R., Venzac, H., Villani, P., Laj, P., Aalto, P., Ogren, J. A., Swietlicki, E., Williams, P., Roldin, P., Quincey, P., Hüglin, C., Fierz-Schmidhauser, R., Gysel, M., Weingartner, E., Riccobono, F., Santos, S., Grüning, C., Faloon, K., Beddows, D., Harrison, R., Monahan, C., Jennings, S. G., O'Dowd, C. D., Marinoni, A., Horn, H.-G., Keck, L., Jiang, J., Scheckman, J., McMurry, P. H., Deng, Z., Zhao, C. S., Moerman, M., Henzing, B., de Leeuw, G., Löschau, G., and Bastian, S.: Mobility particle size spectrometers: harmonization of technical standards and data structure to facilitate high quality long-term observations of atmospheric particle number size distributions, Atmos. Meas. Tech., 5, 657–685, doi:10.5194/amt-5-657-2012, 2012.

Winker, D. M., Tackett, J. L., Getzewich, B. J., Liu, Z., Vaughan, M. A., and Rogers, R. R.: The global 3-D distribution of tropospheric aerosols as characterized by CALIOP, Atmos. Chem. Phys., 13, 3345–3361, doi:10.5194/acp-13-3345-2013, 2013.

Young, L.-H., Benson, D. R., Montanaro, W. M., Lee, S.-H., Pan, L. L., Rogers, D. C., Jensen, J., Stith, J. L., Davis, C. A., Campos, T. L., Bowman, K. P., Cooper, W. A., and Lait, L. R.: Enhanced new particle formation observed in the northern mid-

latitude tropopause region, J. Geophys. Res., 112, D10218, doi:10.1029/2006JD008109, 2007.

Yurkin, M. A. and Hoekstra, A. G.: The discrete dipole approximation: An overview and recent developments, J. Quant. Spectrosc. Ra., 106, 558–589, doi:10.1016/j.jqsrt.2007.01.034, 2007.

Yurkin, M. A. and Hoekstra, A. G.: The discrete-dipole-approximation code ADDA: Capabilities and known limitations, J. Quant. Spectrosc. Ra., 112, 2234–2247, doi:10.1016/j.jqsrt.2011.01.031, 2011.

Zaizen, Y., Okada, K., Ikegami, M., Sawa, Y., and Makino, Y.: Number-size distributions of aerosol particles in the free troposphere over the Northwestern Pacific Ocean – influence of Asian outflow and tropical air transport, J. Meteorol. Soc. Jpn., 82, 1147–1160, 2004.